Rewriting Process of Lower Electrical Resistance Lines on TiO_2 Film using Methods of Whitening with CW Fiber Laser and Darkening with Femtosecond Laser†

TSUKAMOTO Masahiro*, MURAKI Yu, SHINONAGA Togo***, YOSHIDA Minoru**, TAKAHASHI Masanari**** and ABE Nobuyuki***

Abstract

Rewriting process of lower electrical resistance lines on a titanium dioxide (TiO_2) film was developed. In this process, lower electrical resistance lines were written on a TiO_2 film without producing surface topography changes by femtosecond laser irradiation. By heating with a CW fiber laser under air, the electrical resistance of these lines was retained to the higher resistance with no topography changes. This result indicated that the lines could be erased by the local heating method under air. When the erasing-treated area was irradiated with a femtosecond laser, the lower electrical resistance lines could be rewritten with no topography changes of the film surface.

KEY WORDS: (Femtosecond Laser), (CW Fiber Laser), (Titanium Dioxide), (Aerosol Beam)

1. Introduction

The femtosecond laser is an attractive tool for creation of new materials' functions, such as three dimensional optical memories [1-3], photonic crystals [4], waveguide formation [5, 6], refractive-index modification [7-11], periodic nanostructures formation [12-15] and lower electric resistance lines formation [16]. Electric resistance of the lines could be varied by controlling the laser fluence. By the laser focusing spot scanning on the TiO_2 film, patterning of the line was performed. Thus, electric circuits can be written on the film with the laser.

TiO_2 is widely used in environmental cleaning because of its photocatalytic properties. This photocatalytic property enables decomposition of organic matter such as bacteria, mold, and odors [17, 18]. In our previous study, darkening of TiO_2 film surfaces and reduction of their electrical resistance were induced by femtosecond laser irradiation [16]. Darkening could be generated without changing the topography of the film's surface. Thus, the writing process of lower electrical resistance lines on the film could be performed using a method of darkening with a femtosecond laser. It is generally believed that laser-induced oxygen deficiencies in TiO_2, resulting in formation of TiO or Ti, may be the reason for the darkening [16]. Heating at the temperature under melting point is a useful method to repair the oxygen deficiencies. It was reported that the darkened lines on the film formed by femtosecond laser irradiation was whitened by heating with an electric furnace [19]. Then, electrical resistance of darkened lines was increased. After the heating process with an electric furnace, the whitened lines on the film were darkened again by femtosecond laser irradiation. However, wholly darkened lines were whitened by heating with electric furnace because whole area of the film was heated. Continuous wave (CW) fiber laser is one of the useful tools for local heating of materials [20]. Local areas of darkened lines could be whitened by heating with the CW fiber laser. Rewriting process of lower electrical resistance lines on the film can be promoted using a method of both darkening with the femtosecond laser and whitening with the CW fiber laser.

In this study, we developed the rewriting processes of lower electrical resistance lines on the TiO_2 films. The films were formed by the method with an aerosol beam [21, 22]. An aerosol beam used in the experiment was composed of TiO_2 particles and helium (He) gas. The darkened area was created on the films with a femtosecond laser. After the writing process by darkening, the film was heated with a CW fiber laser

† Received on December 26, 2011
* Associate Professor
** School of Science and Engineering, Kinki University
*** Graduate Student
**** Osaka Municipal Technical Research Institute
Transactions of JWRI is published by Joining and Welding Research Institute, Osaka University, Ibaraki, Osaka 567-0047, Japan

under air to whiten the darkened area, which was an erasing process of lower electrical resistance area without changing of the film surface topography. Then, the film surface and its electric resistance were observed and measured. After the erasing process, the whitened area was irradiated with a femtosecond laser again to rewrite the darkened and lower electrical resistance lines on the films without producing surface topography changes.

2. Experimental

Schematic diagram of the experimental setup for femtosecond laser irradiation on the TiO_2 film surface and schematic diagrams of writing with the femtosecond laser, erasing with CW fiber laser and rewriting with the femtosecond laser on the TiO_2 film surface are shown in **Figs. 1(a), (b), (c) and (d)**, respectively. The wavelength, pulse duration, repetition rate and beam diameter of the femtosecond laser were 775 nm, 150 fs, 1 kHz, and approximately 4 mm, respectively. An attenuator to reduce the output energy of the laser was composed of polarizing filters.

The films were formed in area of 10 × 10 mm^2 on the surface of the glass plate with an aerosol beam [21, 22]. An aerosol beam consists of the anatase type TiO_2 particles with a size of about 200 nm and He gas. The thickness of the film was about 5 μm. XRD patterns of (a) TiO_2 film and (b) TiO_2 powder are shown in **Fig. 2**. As indicated in Fig. 2, anatase type crystalline structures were retained throughout the film formation. In the experiments for production of darkened area, the laser beam was focused onto the film surface by a lens with a 100-mm focal length and the film's position was controlled using XY stages connected to a computer. To produce the darkened lines on the film, X stage was moved at the scanning velocity of 1 mm/s during the femtosecond laser irradiation as shown in Fig. 1 (b). The Gaussian laser beam had a diameter of 250 μm (at the $1/e^2$ intensity points) on the film. The laser fluence was varied in the range of 30 to 70 mJ/cm^2 with the period of 10 mJ/cm^2. The electrical resistances were measured by a two-terminal method using two probes (two-probe method), a constant-voltage source, and an ammeter. Steel probes with a tip diameter of about 30μm were used. The two probes were both located along a laser-scanned line. The distance between the probes was 1 mm and a voltage of 60 V was applied between the two tips. The electrical resistances were determined by measuring the electrical current between the two probes. The raw TiO_2 films (not irradiated with the femtosecond laser) had an electrical resistance too large to measure by our two-probe method.

The films after the femtosecond laser irradiation shown in Figs 1(b) were heated by CW fiber laser irradiation, as shown in Fig. 1(c), to whiten the darkened lines. The wavelength and maximum power of CW fiber laser is 1076 nm and 100 W, respectively. To erase the darkened lines on the film, the CW fiber laser beam was focused onto the film surface by a lens with a 250 mm focal length. X stage was moved at the scanning velocity

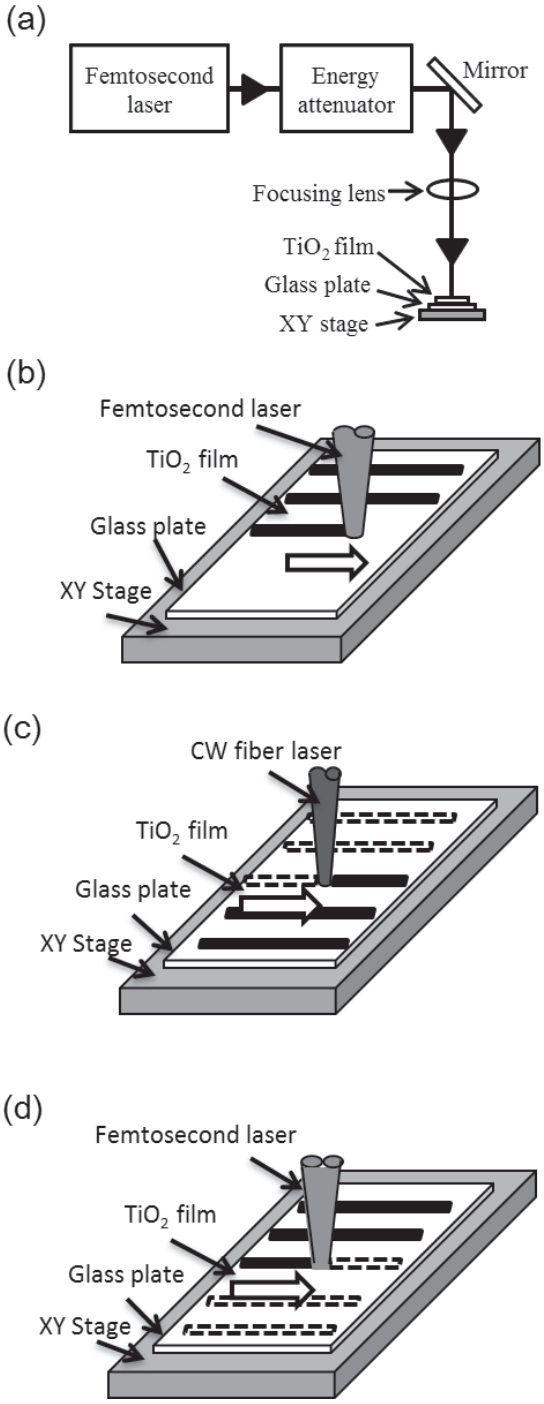

Fig. 1 (a) Schematic diagram of experimental setup for writing and rewriting of lower electrical resistance lines and area on TiO_2 film with a femtosecond laser. (b) Scanning direction of the laser focusing spot for writing with the femtosecond laser, (c) whitening with the CW fiber laser and (d) rewriting with the femtosecond laser.

of 1 mm/s during the CW fiber laser irradiation as shown in Fig. 1 (c). The Gaussian laser beam had a diameter of 550 μm (at the $1/e^2$ intensity points) on the film. The laser intensity of CW fiber laser was 1.8×10^3 W/cm^2. The area whitened by the heating with CW fiber laser was

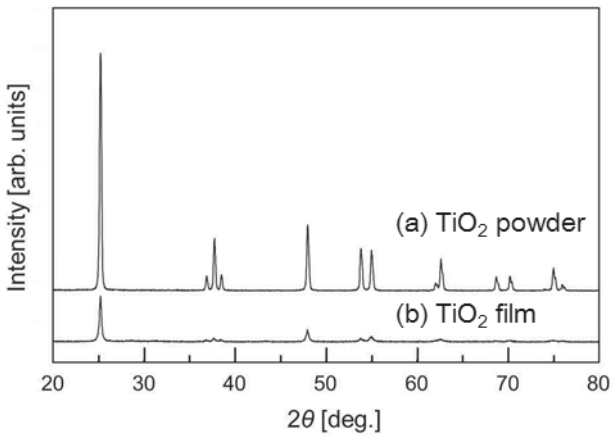

Fig. 2 XRD patterns of (a) TiO_2 powder and (b) TiO_2 film.

irradiated with the femtosecond laser at the laser fluence in the range of 30 to 70 mJ/cm^2 with the period of 10 mJ/cm^2, to rewrite the lower electrical resistance lines as shown in Fig. 1 (d). The surface morphology of the films after the femtosecond laser and the CW fiber laser irradiation was observed with an optical microscope, a scanning electron microscope (SEM).

3. Results and Discussion

Optical images of the film surface irradiated with the femtosecond laser at the laser fluence of 30 to 70 mJ/cm^2 with the period of 10 mJ/cm^2 were shown at a1-a5 in **Fig. 3 (a)**. Local areas of the film were darkened at various laser fluences, as shown at a1-a5 in Fig. 3 (a). **Figure 3 (b)** indicates that optical images of the film surfaces after heating with the CW fiber laser at the laser intensity of 1.8×10^3 W/cm^2. The darkened lines formed by femtosecond laser irradiation at various laser fluences were whitened after CW fiber laser irradiation, as shown at b1-b5 in Fig. 3 (b). Optical images of the darkened lines produced by femtosecond laser irradiation on the whitened area at the laser fluence of 30 to 70 mJ/cm^2 with the period of 10 mJ/cm^2 are shown at c1-c5 in **Fig. 3 (c)**. Figure 3 (c) shows that, by the femtosecond irradiation, the darkened lines could be written on the whitened area.

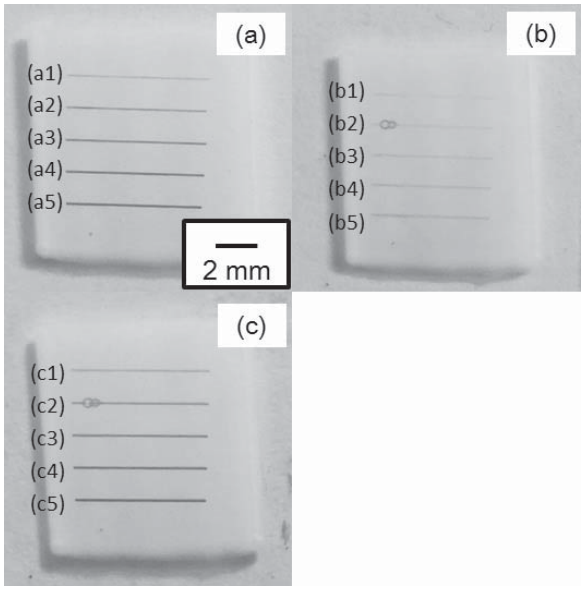

Fig. 3 (a) Darkened lines in optical image were written on the film with a femtosecond laser at the laser fluence of 30～70 mJ/cm^2 with the period of 10 mJ/cm^2. (b) Whitened the darkened lines in optical image were erased with a CW fiber laser at the laser intensity of 1.8×10^3 W/cm^2. (c) Darkened lines in optical image were rewritten on the film with a femtosecond laser at the laser fluence of 30～70 mJ/cm^2 with the period of 10 mJ/cm^2.

SEM image of the films' surface is shown in **Fig. 4 (a)**. SEM images of the films' surface shown at a4 in Figs. 3 (a), b4 in Figs. 3 (b) and c4 in Figs. 3 (c) are

Fig. 4 SEM images of law TiO_2 film surface (a) and laser irradiated areas after writing with femtosecond laser (b), whitening with CW fiber laser (c) and rewriting with femtosecond laser (d), respectively.

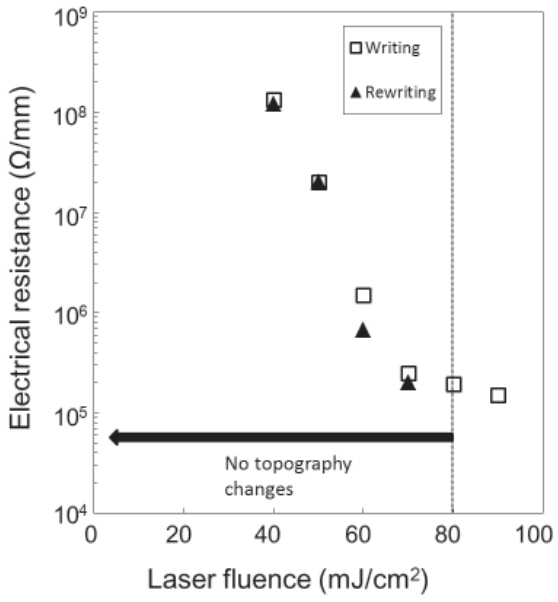

Fig. 5 Electrical resistance along a 1 mm length of lines formed on the film as a function of the laser fluence. Square and triangle indicate electrical resistances of written lines on the film and rewritten lines on the erasing-treated film with femtosecond laser, respectively.

shown in **Figs. 4 (b), (c) and (d)**, respectively. As indicated in Figs. 4 (a), (b), (c) and (d), topography of the films' surfaces was not changed through the writing with the femtosecond laser, whitening with the CW fiber laser and rewriting with the femtosecond laser.

Squares and triangles in **Fig. 5** show the electrical resistances of the darkened lines shown in Figs. 3 (a) and (c) at various femtosecond laser fluences, respectively. As shown with squares in Fig. 5, the electrical resistances of the darkened lines were decreased as the laser fluence was increased. This result was the same as that obtained in Ref. [16]. The electrical resistances of the darkened lines formed on the whitened area by the femtosecond laser irradiation again was also decreased as the laser fluence was increased as shown with triangles in Fig. 5. Results shown in Figs. 3 and 5 indicate that rewriting of lower electrical resistance lines on the film could be promoted by the femtosecond and CW fiber laser irradiation.

4. Summary

Rewriting technology of lower electric resistance lines on the TiO_2 film could be developed using the method of whitening, erasing, by the local heating with a CW fiber laser and darkening, writing, by the femtosecond laser irradiation. The darkened and the lower electric resistance lines on the film could be erased by the heating with the CW fiber laser under air. They could be rewritten on the erasing-treated film by the femtosecond laser irradiation.

Reference

1) Y. Kawata, H.Ishitobi and S.Kawata: Opt. Lett., 23 (1998) 756-758.
2) G. Zhou and M. Gu: Appl.Phys. Lett., 87 (2005) 241107.
3) S. Juodkazis, M. Sudzius, V. mizeikis, H. Misawa, E.G.Gamaly, Y.Liu, O.A.Louchev and K.Kitamura: Appl. Phys. Lett., 89 (2006) 062903.
4) G. Zhou and M. Gu: Opt. lett., 31 (2006) 2783-2785.
5) L. Gui, B. Xu and T.C.Chong: IEEE Photon. Technol. Lett., 16 (2004) 1337 - 1339.
6) J. Burghoff, S. Nolte and A. Tuennermann: Appl. Phys. A: Mater. Sci. Process., 89 (2007) 127-132.
7) K. Buse, A. Adibi and D. Psaltis: Nature (London), 393 (1998) 665-668.
8) A. Adibi, K.Buse and D. Psaltis: J. Opt. Soc. Am. B, 18 (2001) 584-601.
9) N. V. Kukhtarev, G. E. Dovgalenko and V. N. Starkov: Appl. Phys. A , 33 (1984) 227-230.
10) B. Sturman, M. Carrascosa and F. Agullo-Lopez: Phys. Rev. B, 78 (2008) 245114.
11) N. Kukhtarev, V. Markov and S. Odulov: Zh. Tech. Fiz., 50 (1980) 1905.
12) M. Hashida, M. Fujita, M. Tsukamoto, A. F. Semerok, O. Gobert, G. Petite, Y. Izawa and J. F. Wagner: Proc. of SPIE, 4830 (2003) 452-457.
13) M. Tsukamoto, K. Asuka, H. Nakano, M. Hashida, M. Katto, N. Abe and M. Fujita: VACUUM, 80 (2006) 1346-1350.
14) M. Tsukamoto, T. Kayahara, H. Nakano, M. Hashida, M. Katto, M. Fujita, M. Tanaka and N. Abe: J. Phys., Conf. Ser., 59 (2007) 666-669.
15) H. Honda, M. Tsukamoto, N. Abe, T. Shinonaga and M. Fujita: Ceramic Transactions, 219 (2010) 299-303.
16) M. Tsukamoto, N. Abe, Y. Soga, M. Yoshida, H. Nakano, M. Fujita and J. Akedo: Appl. Phys. A, 93 (2008) 193-196.
17) A. Fujishima and K. Honda: Bull. Chem. Soc. Jpn., 44 (1971) 1148-1150.
18) A. Fujishima and K. Honda: Nature, 238 (1972) 37-38.
19) M. Tsukamoto, T. Shinonaga, N. Abe, M. Takahashi, M. Yoshida, H. Nakano and M. Fujita: JLMN, 6, 2 (2011) 164-167.
20) M. Tsukamoto, S. Yagi, T. Shibayanagi, M. Fujita, N. Abe: proceeding of ICALEO 2009 (2009) 1210-1213.
21) M. Tsukamoto, T. Fujihara, N. Aba, S. Miyake, M. Katto, T. Nakayama and J. Akedo: Jpn. J. Appl. Phys., 42 (2003) L120-L122.
22) M. Tsukamoto, M. Mori, S. Baba, N. Abe and J. Akedo: Transactions of the Materials Research Society of Japan, 30, 4 (2005) 1013-1016.

Bonding process of Cu/Cu joint using Cu nanoparticle paste†

NISHIKAWA Hiroshi*, HIRANO Tomoaki**, TAKEMOTO Tadashi***

Abstract

High-temperature bonding, or joining, is a key technology for electronic component assembly and other high-temperature applications. Recently, focusing on the sintering behavior of nanoparticles, the joining process using a nanoparticle paste has been proposed as an alternative to soldering for high-temperature applications. In this study, Cu nanoparticle paste was used to join two Cu discs, and the effect of heating conditions on the joint strength of the Cu-to-Cu joint was investigated. Joining using Cu nanoparticle paste was successfully achieved, and joints that were bonded at 673 K for 300 s under nitrogen atmosphere showed high shear strength.

KEY WORDS: (High-temperature joining), (Cu nanoparticle paste), (Cu-to-Cu joint), (Shear strength), (high-temperature applications)

1. Introduction

The European Restriction of Hazardous Substances (RoHS) directive currently exempts the used of high-lead-containing solders for high-temperature soldering, as high-temperature soldering is a key technology for electronic component assembly and other high-temperature applications. However, there is no guarantee that the exemption will last. A strong drive thus exists to find lead-free alternatives for high-temperature joining processes. Research is needed to establish and characterize a new joining process for high-temperature applications. Several materials and joining processes have been proposed as alternatives to high-lead-containing solders. For example, Au-, Zn- and Bi-based alloys have been investigated for use as lead-free solder, but their widespread use is unlikely because of their inferior properties and high costs [1-8]. New joining processes involving thin film joining process using evaporated films and sintering process using particles have also been proposed as solder alternatives [9-11].

Metals such as Ag, Cu and Au have high electrical and thermal conductivities and exhibit limited fatigue. These metals tend to have high melting points. These properties make them suitable for high-temperature joining process. For instance, one candidate process that might be applicable for joining at lower temperature is sintering. Standard sintering procedures still require relatively high joining temperatures, although the sintering temperature of a metal particle is below its melting point. Related to using nanoparticles, it is well known that metal nanoparticles sinter and melt at temperatures lower than that for the bulk metal. The sintering behavior of nanoparticles is of significant interest.

Furthermore, the sintering behavior of metallic nanoparticles has been exploited to write electronic circuits and join components to substrate [12-17]. For example, Ide et al. [13] reported achieving Cu-to-Cu joining using Ag metallo-organic nanoparticles at a low bonding temperature (573 K) and a bonding pressure of 1 or 5 MPa; the shear strength of the resulting joints was 25-40 MPa. Bonding was believed to occur because of the large surface energy contributed by the nanoparticles. As the latest work for low temperature bonding using Ag nanoparticles, Hu et al. [16] reported that robust bonding of Cu wire to Cu pads on polyimide was achieved at 373 K through solid state sintering of Ag nanoparticle and metallic bonding of Ag to Cu substrates. Using the sintering behavior of Cu nanoparticles, Jang et al. [17] reported using Cu nanoparticles as ink to print a conductive Cu pattern directly on flexible polyimide substrates using their own functional materials and printing system. However, the microstructure in the bottom of the film was not completely dense and the achieved line exhibited higher resistance than a conventional conductive line.

Cu nanoparticles seem particularly promising for joining materials because of their low resistivity, low cost and good electromigration performance. Accordingly, our

† Received on December 26, 2011
* Associate Professor
** Graduate Student
*** Specially Appointed Professor

Transactions of JWRI is published by Joining and Welding Research Institute, Osaka University, Ibaraki, Osaka 567-0047, Japan

research group has proposed a joining process for high-temperature applications that uses Cu nanoparticle paste as an alternative to solder. In this study, the effect of heating conditions on the joint strength of a Cu-to-Cu joint formed using Cu nanoparticle paste has been investigated to obtain high joint strength.

2. Experimental

The paste used in this study consisted of Cu nanoparticles and organic solvent, for a metal content of about 60 mass%. Cu nanoparticles were synthesized by a chemical reduction method in solution. A glycol system was used as organic solvent to prevent oxidation of Cu nanoparticles. Nanoparticle diameters were in the ranges of 10 to 20 nm. The thermal characteristics of the paste were measured by differential thermal analysis (DTA) and thermogravimetry (TG) at a heating rate of 0.17 K/s in air and under a nitrogen atmosphere.

The two different-sized oxygen-free Cu specimens were used for the joining experiment. The faying surfaces of the specimens were polished with with 2000-grit SiC paper and 1 μm diamond paste, then soaked in ethanol solution for 300 s. Just before bonding, the specimens were soaked in hydrochloric acid and cleaned with distilled water and ethanol solution. Cu nanoparticle paste was applied to the faying surface of the φ10 mm Cu specimen to a thickness of 150 μm, and then the φ3 mm Cu specimen was set on top.

Cu-to-Cu disc specimens so created were bonded by heating in a furnace. Bonding was performed in a two-step heating process. For two-step heating, specimens were preheated for various times (60, 300, 600, 1800 s) under normal pressure at the following temperatures: 363, 393, 423, 453, 483, 513, and 543 K; then they were heated for various heating times (60, 300, 1800, 3600 s) under joining pressure of 15 MPa at the following temperatures: 553, 593, 633, and 673 K. The joining atmosphere was air or a nitrogen atmosphere.

The shear test method was used to investigate the joint strength of the disc joints. The shear strengths of three joints for each joining condition were measured at a shear strain rate of 0.017 mm/s. The strength was estimated by the average of three trials. After shearing, the fracture surfaces were observed by scanning electron microscopy (SEM).

3. Results and discussion

Figure 1 shows DTA and TG curves for Cu nanoparticle paste during heating at a rate of 0.17 K/s in air and under a nitrogen atmosphere. For heating both in air and under nitrogen atmosphere, a first mass loss is evident at 380-450 K, attributable to decomposition of the solvent, and a second loss of mass is evident at around 570 K. The DTA curves show clear exothermal behavior, at much higher intensity in air than under nitrogen atmosphere. The second loss of mass can be attributed to decomposition of the protective agent that was present in the nanoparticles to prevent self-cohesion. The TG curves in air and under nitrogen atmosphere are essentially identical until 670 K, after which a gain in mass is evident in air but not under nitrogen atmosphere, perhaps attributable to oxidation of the nanoparticles.

The Cu-to-Cu disc joints using Cu nanoparticle paste were made using two-step heating process. To investigate the effect of joining atmosphere on the joint strength, the disc joints using Cu nanoparticle paste were made in air and under a nitrogen atmosphere. **Figure 2** shows the effect of joining atmosphere on the shear strength of the disc joints. The preheating was performed for 300 s under normal pressure at 423 K, and then heating was performed for 300 s at 673 K. The shear strength under

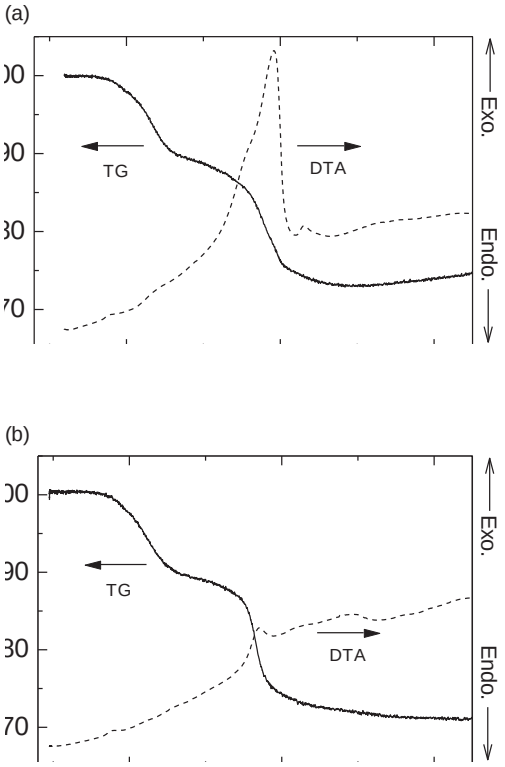

Fig. 1 DTA and TG curves of Cu nanoparticle paste under heating rate of 0.17 K/s in Air (a) and N2(b).

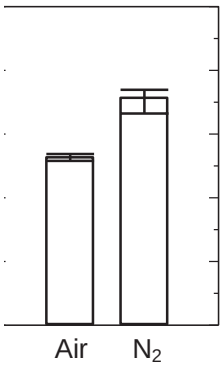

Fig. 2 Effect of joining atmosphere on shear strength of joints using Cu nanoparticle paste. (Preheating temperature: 423 K, preheating time 300 s, heating temperature: 673 K, heating time 300 s, bonding pressure: 15 MPa)

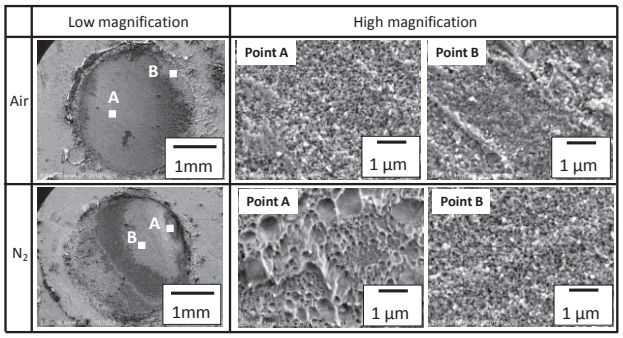

Fig. 3 SEM images of typical fracture surface of joints in air and N_2. (Preheating temperature: 423 K, preheating time 300 s, heating temperature: 673 K, heating time 300 s, bonding pressure: 15 MPa)

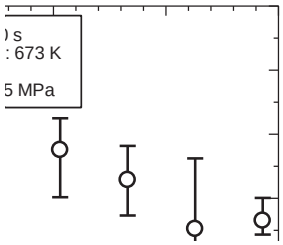

Fig. 4 Effect of preheating temperature for 300 s on shear strength of joints in N_2. (Preheating time: 300 s, heating temperature: 673 K, heating time: 300 s, bonding pressure: 15 MPa)

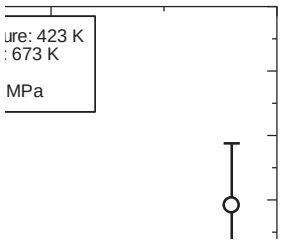

Fig. 5 Effect of preheating time at 423 K on shear strength of joints in N_2. (Preheating temperature: 423 K, heating temperature: 673 K, heating time: 300 s, bonding pressure: 15 MPa)

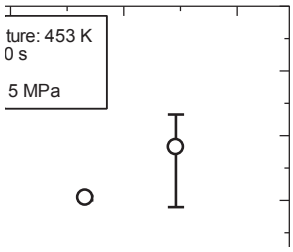

Fig. 6 Effect of heating temperature for 300 s on shear strength of joints in N_2. (Preheating temperature: 453 K, preheating time: 300 s, heating time: 300 s, bonding pressure 15 MPa)

the nitrogen atmosphere was higher than that in air. The strength is ~40 MPa. This result suggests that it is important to prevent oxidation of Cu nanoparticles during heating. To investigate the difference of the joint strength related to the atmosphere, the fracture surface after the shear test was observed. **Figure 3** shows SEM images of the fracture surface of disc joints in air and under the nitrogen atmosphere. For heating both in air and under the nitrogen atmosphere, distinctive fracture surfaces are evident in joints bonded at 673 K. Especially for heating under the nitrogen atmosphere, the nanoparticles have sintered, and an elongated dimple structure is partially observable on the fracture surface of the joints. On the other hand, for heating in air, the spherical shape made from Cu nanoparticles is retained in all area. This result suggests that Cu nanoparticle sintering progresses effectively under nitrogen atmosphere.

The Cu-to-Cu disc joints using Cu nanoparticle paste were made under the various preheating and heating conditions under a nitrogen atmosphere. **Figure 4** shows the effect of the preheating temperature on the shear strength of the disc joints. The preheating was performed for 300 s under normal pressure at various temperatures, and then heating was performed for 300 s at 673 K. For preheat process, the temperature < 500 K have no effect on shear strength. For preheat temperatures of 513 and 543 K, shear strength clearly decreases relative to its values at lower temperatures. This result may be attributable to gradual nanoparticle sintering during preheating process, causing them to assume a size that prevents subsequent sintering during the second heating step at 673 K. **Figure 5** shows the effect of the preheating time on the shear strength of the disc joints. The preheating was performed for various times under normal pressure at 423 K, and then heating was performed for 300 s at 673 K. The maximum shear strength was found at 300 s. For preheat time of 1800 s, shear strength clearly decreases relative to its values at shorter time. This result may be also attributable to gradual nanoparticle sintering during preheating process.

Figure 6 shows the effect of the heating temperature on the shear strength of the disc joints. The preheating was performed for 300 s under normal pressure at 453 K, and then heating was performed for 300 s at various temperatures. The shear strength of the disc joints increases with increasing heating temperature; at 553 and 593 K it is < 15 MPa and at 673 K, which is higher than the decomposition temperature of the protective agent, it

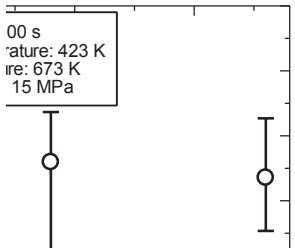

Fig. 7 Effect of heating time at 673 K on shear strength of joints in N_2. (Preheating temperature: 423 K, preheating time: 300 s, heating temperature: 673 K, bonding pressure: 15 MPa)

is < 35 MPa. The thermal characteristics of the paste strongly affect the relationship between heating temperature and joint strength. **Figure 7** shows the effect of the heating time on the shear strength of the disc joints. The preheating was performed for 300 s under normal pressure at 423 K, and then heating was performed for various times at 673 K. the heating time > 60 s have little effect on shear strength.

4. Conclusions

In this study, a joint process using Cu nanoparticle paste was developed as a replacement for high-lead containing solder for high-temperature applications. Especially, the effect of heating conditions on the shear strength of Cu-to-Cu disc joints using Cu nanoparticle paste was investigated. The main results are as follows:

(1) Joints that were bonded under a nitrogen atmosphere at 673 K for 300 s under a joining pressure of 15 MPa showed high shear strength (～40MPa), demonstrating the successful use of Cu nanoparticle paste to form joints. Under the nitrogen atmosphere, the nanoparticles in the paste became effectively sintered, forming an elongated dimple structure that was partially observable on the fracture surface of the joint.

(2) Joining conditions such as preheating temperature and heating temperature significantly affect the shear strength of a joint.

References

1) Chidambaram V, Hattel J, Hald J., Design of lead-free candidate alloys for high-temperature soldering based on the Au-Sn system, Materials and Design, **31** (2010)**,** 4638-4645.

2) Liu Y.C, Teo J.W.R, Tung S.K, Lam K.H., High-temperature creep and hardness of eutectic 80Au/20Sn solder, Journal of Alloys and Compounds, **448** (2008) ,340-343.

3) Chidambaram V, Hald J, Hattel J., Development of Au-Ge based candidate alloys as an alternative to high-lead content solders, Journal of Alloys and Compounds, **490** (2010), 170-179.

4) Rettenmayr M, Lambracht P, Kempf B, Tschudin C., Zn-Al based alloys as Pb-free solders for die attach, Journal of Electronic Materials, **31** (2002), 278-85.

5) Kang N, Na H.S, Kim S.J, Kang C.Y., Alloy design of Zn-Al-Cu solder for ultra high temperature, Journal of Alloys and Compounds, **467** (2009), 246-250.

6) Yamada Y, Takaku Y, Yagi Y, Nishibe Y, Ohnuma I, Sutou Y, Kainuma R, Ishida K., Pb-free high temperature solders for power device packaging, Microelectronics Reliability, **46** (2006), 1932-1937.

7) Takashashi T, Komatsu S, Nishikawa H, Takemoto T., Improvement of high-temperature performance of Zn-Sn solder joint, Journal of Electronic Materials, **39** (2010), 1241-1247.

8) Song J. M, Chuang H.Y, Wu Z.M., Interfacial reactions between Bi-Ag high-temperature solders and metallic substrates, Journal of Electronic Materials, **35** (2006), 1041-1049.

9) Zhang Z, Lu G. Q., Pressure-assisted low-temperature sintering of silver paste as an alternative die-attach solution to solder reflow, IEEE Transactions on Electronics Packaging Manufacturing, **25** (2002), 279- 283.

10) McCluskey F.P, Dash M, Wang Z, Huff D., Reliability of high temperature solder alternatives, Microelectronics Reliability, **46** (2006), 1910-1914.

11) Takahashi T, Kamatsu S, Nishikawa H, Takemoto T., Thin film joining for high-temperature performance of power semi-conductor devices, Microelectronics Reliability, **50** (2010), 220-227.

12) Dong H, Moon K.S, Wong C.P., Molecular dynamics study of nanosilver particles for low-temperature lead-free interconnect applications, Journal of Electronic Materials, **34** (2005), 40-44.

13) Ide E, Angata A, Hirose A, Kobayashi K.F., Metal-metal bonding using Ag metallo-organic nanoparticles., Acta Materialia, **53** (2005), 2385-2393.

14) Akada Y, Tatsumi H, Yamaguchi T, Hirose A, Morita T, Ide E., Interfacial bonding mechanism using silver metallo-organic nanoparticles to bulk metals and observation of sintering behavior, Materials Transactions, **49** (2008), 1537-1545.

15) Wakuda D, Kim K.S, Suganuma K., Room temperature sintering of Ag nanoparticles by drying solvent, Scripta Materialia, **59** (2008), 649-652.

16) Hu A, Guo J.Y, Alarifi H, Patane G, Zhou Y, Compagnini G, Xu C.X., Low temperature sintering of Ag nanoparticles for flexible electronics packaging, Applied Physics letters, **97** (2010), 153117.

17) Jang S., Seo Y, Choi J, Kim T, Cho J, Kim S, Kim D., Sintering of inkjet printed copper nanoparticles for flexible electronics, Scripta Materialia, **62** (2010), 258-261.